Science Advances
AAAS

advances.sciencemag.org/cgi/content/full/6/13/eaaz1659/DC1

Supplementary Materials for

Coordinated regulation of infection-related morphogenesis by the KMT2-Cre1-Hyd4 regulatory pathway to facilitate fungal infection

Yiling Lai, Xuan Cao, Jingjing Chen, Lili Wang, Gang Wei*, Sibao Wang*

*Corresponding author. Email: weigang@picb.ac.cn (G.W.); sbwang@sibs.ac.cn (S.W.)

Published 25 March 2020, *Sci. Adv.* **6**, eaaz1659 (2020)
DOI: 10.1126/sciadv.aaz1659

This PDF file includes:

Supplementary Figures

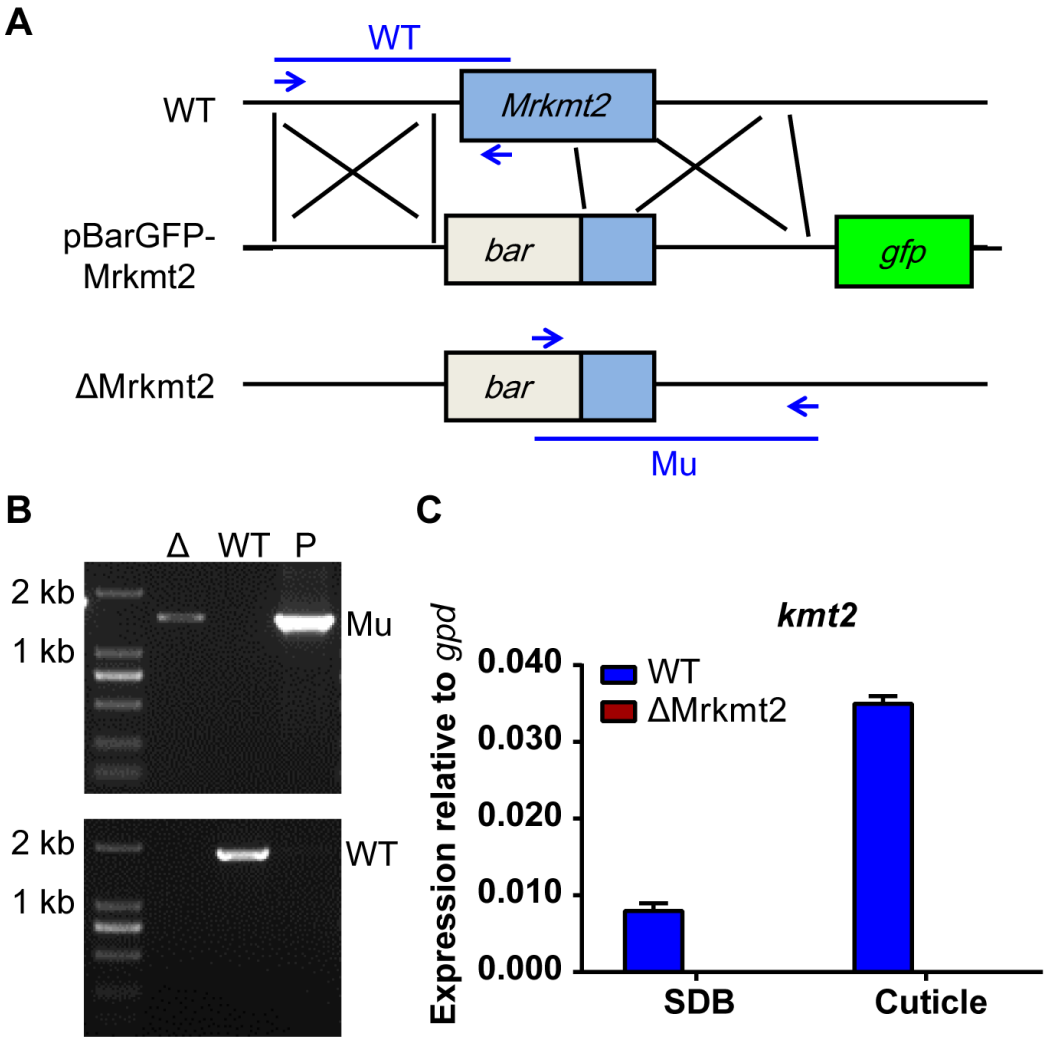

Fig. S1. Disruption of the *Mrkmt2* gene in *M. robertsii* ARSEF 2575. (**A**) Schematic representation of the *Mrkmt2* wild-type (WT) locus and plasmid pBarGFP-Mrkmt2 (containing two regions identical with the *Mrkmt2* reading frame), which was used for gene disruption via double-crossover recombination. Replacement and WT-specific primer combinations and the expected fragments are shown as blue lines. The blue arrows indicate the position and polarity (5′-3′) of primers used for confirmatory polymerase chain reaction (PCR) (**B**) Replacement-specific PCR analysis. The gene targeting was confirmed using primer combinations that amplify a signal only from the recombinant locus (Mu). The absence of a WT-specific signal in the mutant ΔMrkmt2 (Δ) strain and plasmid pBarGFP-Mrkmt2 (P) in the lower image confirms the genetic homogeneity of the mutant. (**C**) *Mrkmt2* expression was verified by quantitative PCR (qPCR) using cDNA from WT and ΔMrkmt2 cultures in the Sabouraud dextrose broth (SDB) and minimal medium (MM) supplemented with 0.8% locust cuticle.

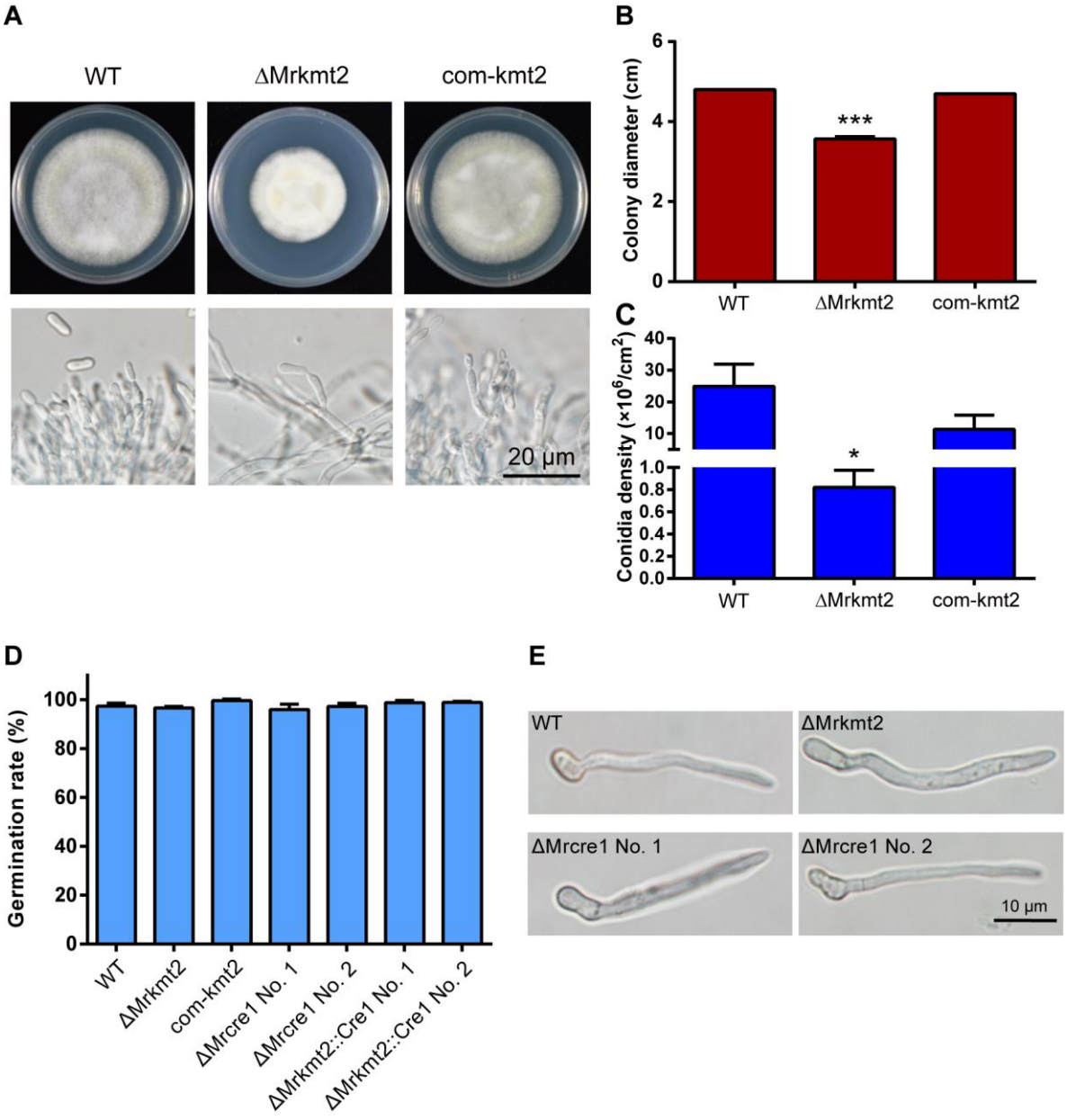

Fig. S2. Growth and conidial germination assay. (**A**) Fungal growth and sporulation assays. (Top) Fungal growth on potato dextrose agar (PDA) plates after 10 d; (bottom) microscopic observations of conidiophores and conidia of the WT, ΔMrkmt2, and com-kmt2 strains examined on day 10 of the corresponding PDA cultures. (**B**) Colony diameter of the WT, ΔMrkmt2, and com-kmt2 strains. (**C**) Conidia production by the WT, ΔMrkmt2, and com-kmt2 strains. The mutant ΔMrkmt2 strain produces significantly less conidia than the WT strain. (**D**) Conidial germination rates of the WT, ΔMrkmt2, com-kmt2, ΔMrcre1, and ΔMrkmt2::Cre1 strains on a hydrophobic surface in plastic plates were measured under a light microscope after incubation at 27 °C for 12 h. 100 conidia per plate were examined. (**E**) Microscopic observation of germ tubes at 12 h post inoculation. Data are shown as mean ±

SD of three technical replicates. Experiments were repeated three times with similar results. Single and triple asterisks represent significant differences determined by Student's *t*-test at $P < 0.05$ and $P < 0.001$, respectively.

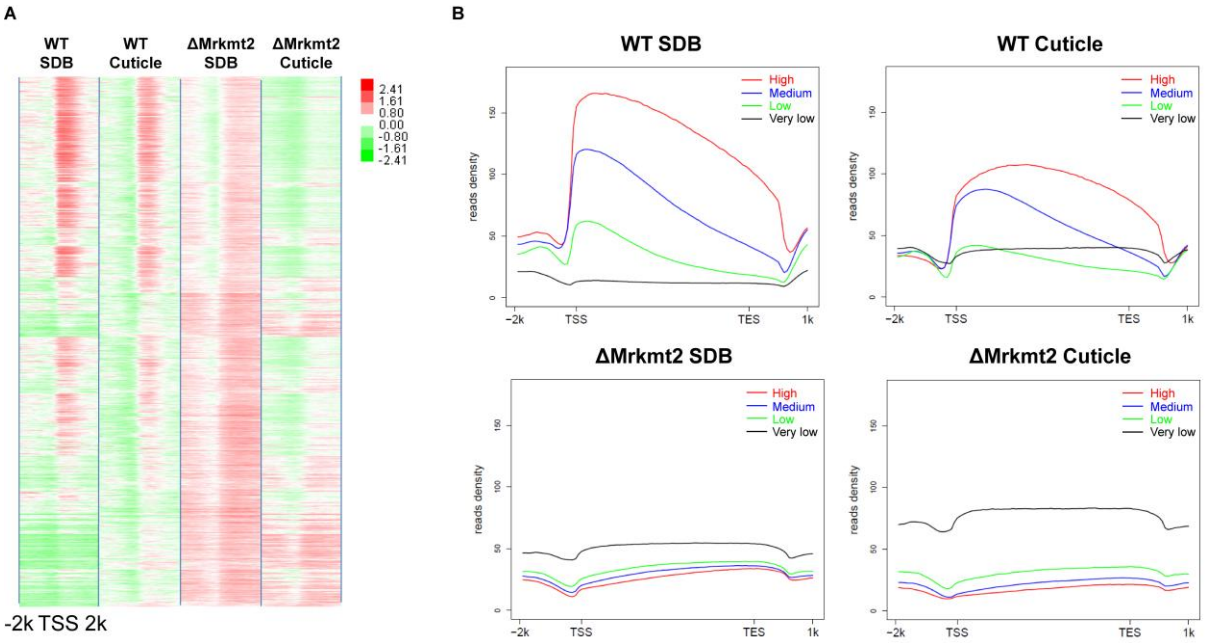

Fig. S3. MrKMT2-mediated H3K4me3 is associated with gene activation. (A) Heatmaps of H3K4me3 states at transcriptional start site (TSS) ± 2 kb. H3K4me3 accumulates mostly near the 5′-region of genes. Red and green indicates high and low level of H3K4me3, respectively. (B) A global view of the relationship between H3K4me3 modification and gene expression. Genes were categorized into four groups based on their expression levels (high, medium, low, very low), and the levels of H3K4me3 (shown as reads density) in each gene group were analyzed. H3K4me3 levels were positively correlated with gene expression levels in the WT strain grown in the SDB and MM medium supplemented with 0.8% locust cuticle. TES, transcriptional end site.

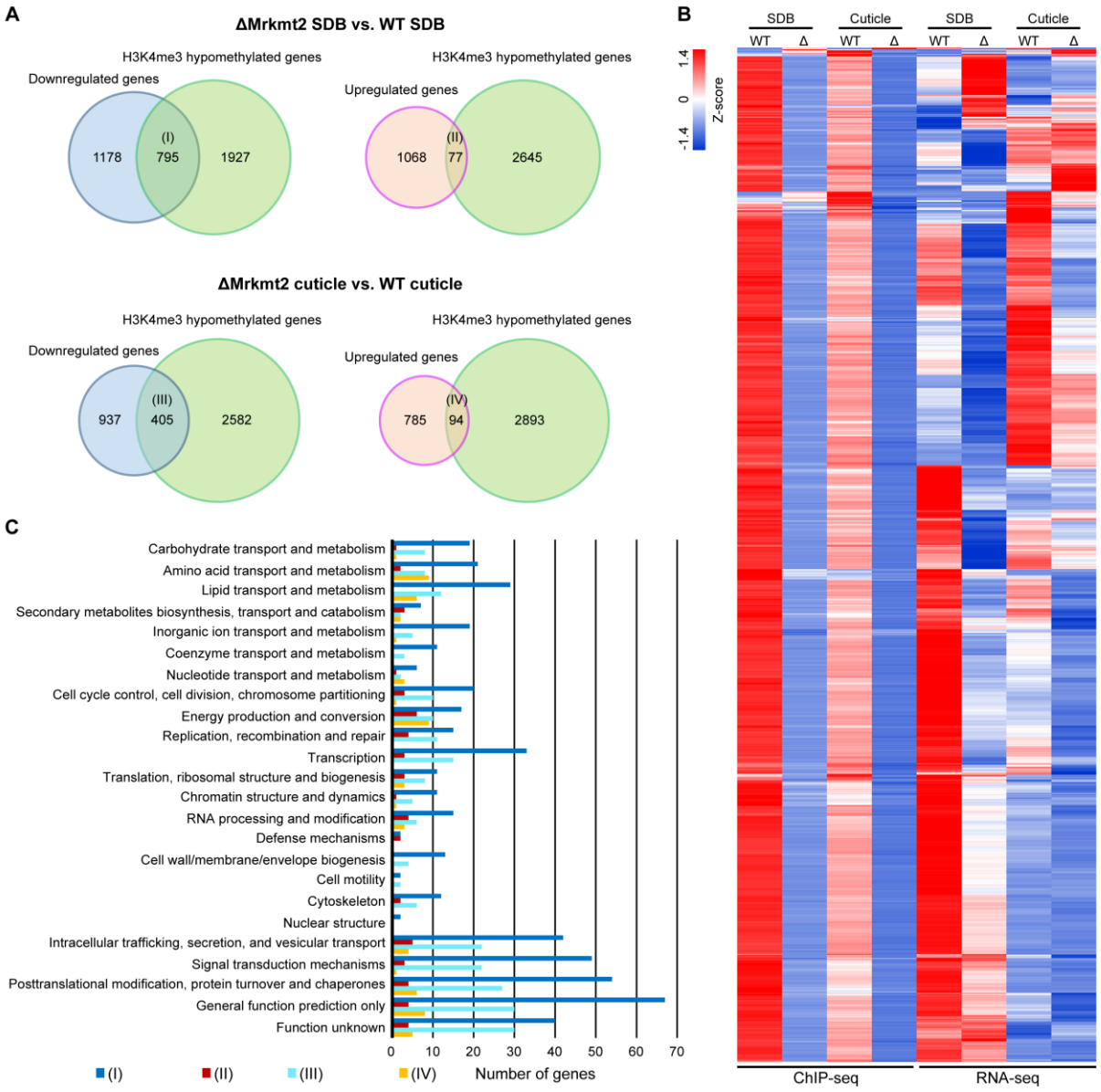

Fig. S4. Characterization of genes transcriptionally regulated by MrKMT2-mediated H3K4me3. (**A**) Venn diagrams showing overlaps of downregulated (1973) or upregulated (1145) genes in ΔMrkmt2 SDB cultures vs. WT SDB cultures [the genes considered (2722) were all H3K4me3-hypomethylated in ΔMrkmt2 SDB cultures]; and overlaps of downregulated (1342) or upregulated (879) genes in ΔMrkmt2 cuticle cultures vs. WT cuticle cultures [the genes considered (2987) were all H3K4me3-hypomethylated in ΔMrkmt2 cuticle cultures]. In total, 795, 77, 405, and 94 genes were identified in the overlapping sets I, II, III, and IV, respectively. Overall, 1150 genes were identified as genes whose expression is directly modulated by MrKMT2-mediated H3K4me3. (**B**) Heat map showing the H3K4me3 enrichment at the promoters (TSS ± 1 kb) of 1150 genes directly modulated by H3K4me3

(left; ChIP-seq) and their corresponding expression patterns (right; RNA-seq). (**C**) KOG functional classification of the overlapping group I, II, III, and IV genes.

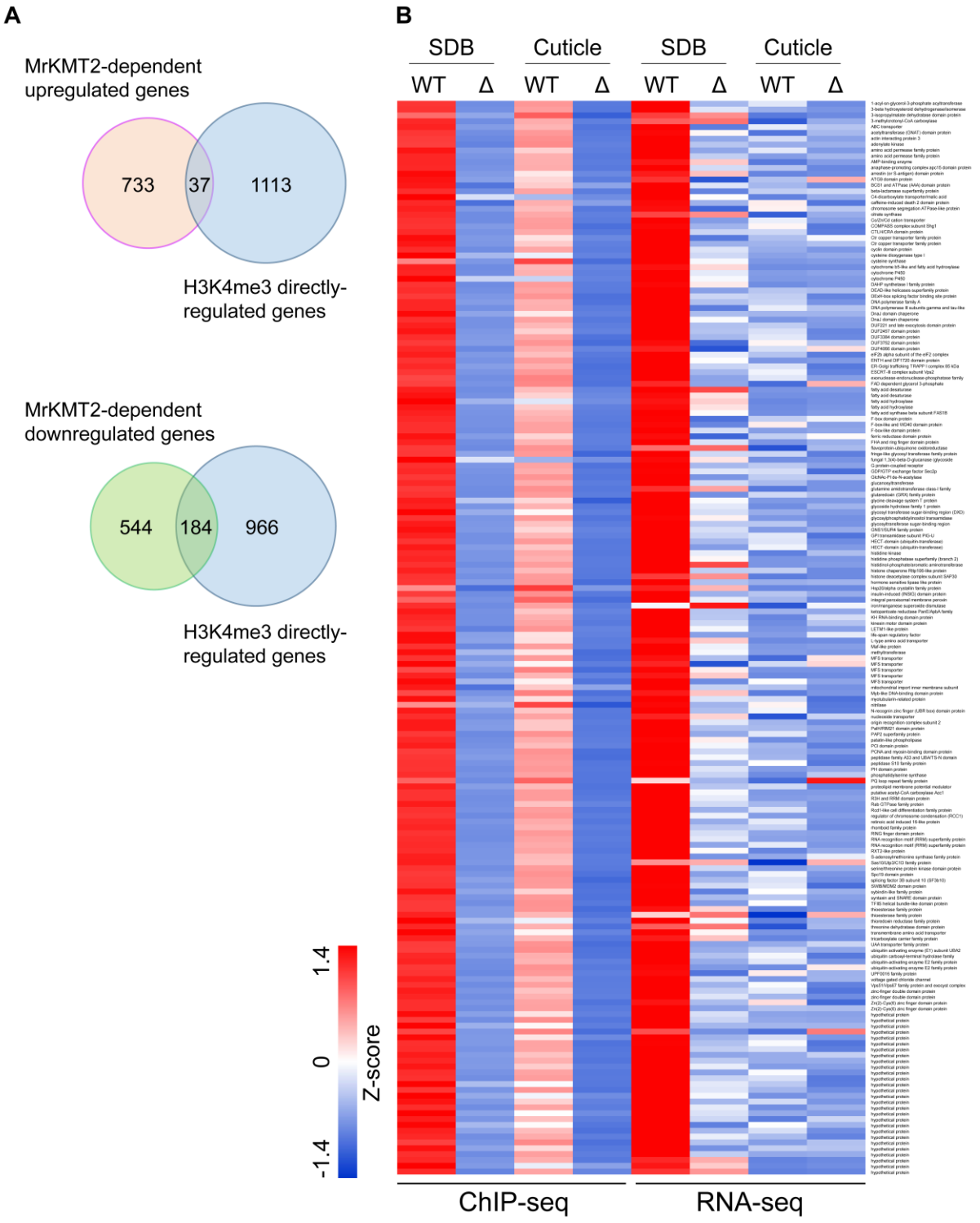

Fig. S5. Characterization of genes directly modulated by H3K4me3 in an MrKMT2-dependent manner. (**A**) Venn diagrams showing overlaps of MrKMT2-dependent upregulated (770) or downregulated (728) genes and genes directly modulated by H3K4me3

(1150). Among 770 MrKMT2-dependent upregulated genes, only 37 genes are directly modulated by H3K4me3; 184 genes are directly modulated by H3K4me3 in 728 MrKMT2-dependent downregulated genes. (**B**) Heat map showing H3K4me3 enrichment at the promoters (TSS ± 1 kb) of 184 directly H3K4me3-modulated genes that are downregulated in an MrKMT2-dependent manner (left; ChIP-seq) and their corresponding expression patterns (right; RNA-seq).

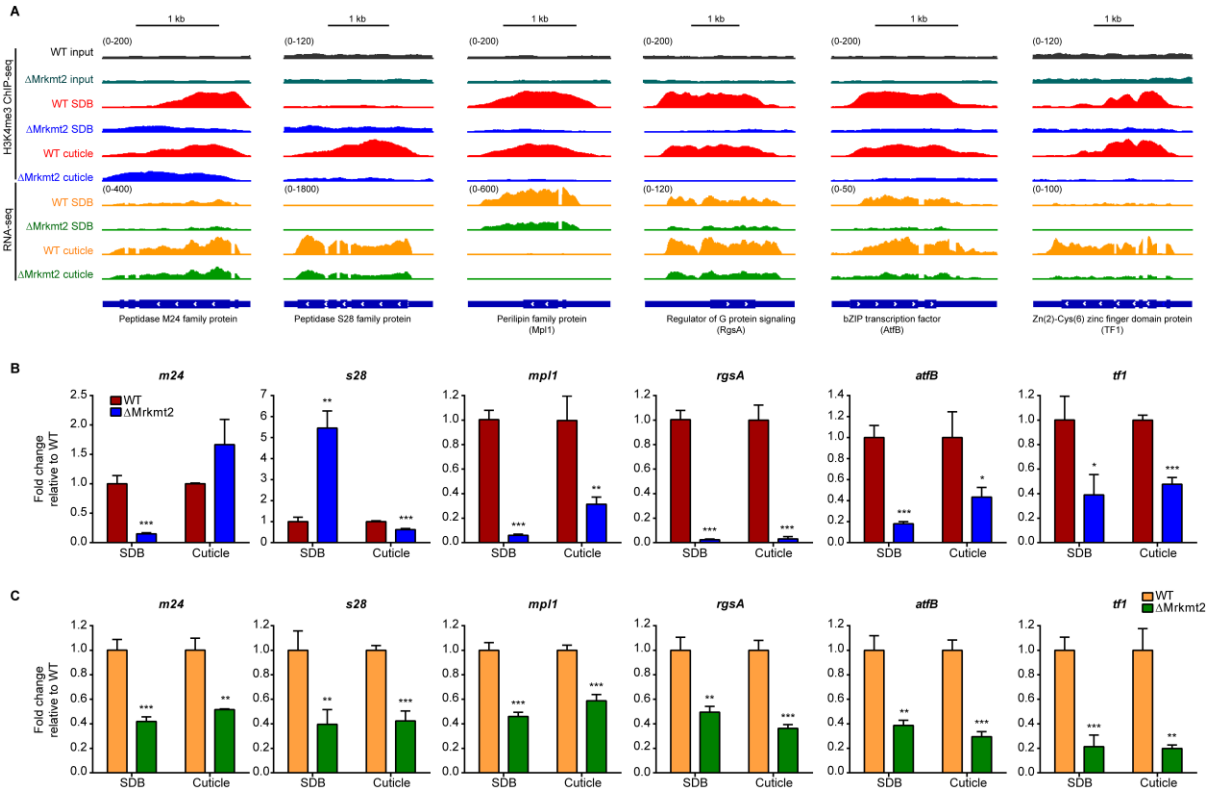

Fig. S6. Six direct gene targets of MrKMT2-mediated H3K4me3. (**A**) A genome browser view showing H3K4me3 signals at the promoters (TSS ± 1 kb) of the six genes, and gene expression in the WT and ΔMrkmt2 strains grown in the SDB and MM medium supplemented with 0.8% locust cuticle. (**B**) ChIP-qPCR validation of ChIP-seq, shown as the fold-change in the signal from immunoprecipitation over the relative input DNA. (**C**) qPCR analysis of the expression levels of the six selected genes in the WT and ΔMrkmt2 strains grown in the SDB and MM medium supplemented with 0.8% locus cuticle. Gene expression in ΔMrkmt2 was normalized to that in WT (taken as 1.0); actin was used as a reference gene. Data are shown as mean ± SD of three technical replicates. Experiments were repeated three times with similar results. Single, double, and triple asterisks represent significant differences determined by Student's *t*-test at $P < 0.05$, $P < 0.01$, and $P < 0.001$, respectively.

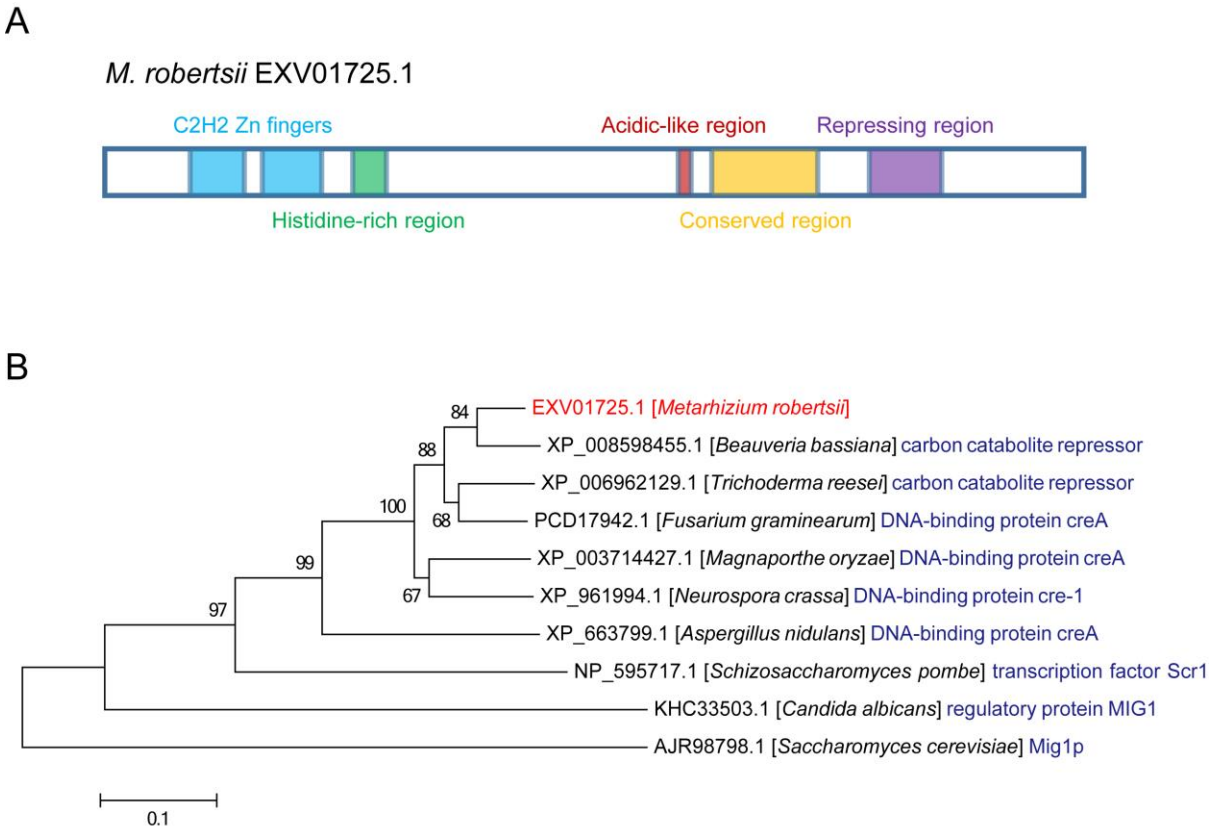

Fig. S7. Characterization of MrCre1 (EXV01725.1). (**A**) Domain structures of MrCre1. MrCre1 was predicted to contain two Cys2His2 zinc-finger domains, a histidine-rich region (HHHHQHHHHHHHQ), an acidic-like region (EDHDD), a conserved region, and a repressing region. (**B**) The phylogenetic relationship of MrCre1 and its homologs shows that MrCre1 shares the highest homology with the *Beauveria bassiana* Cre1 sequence, and is also similar to the Cre1 sequences in *Trichoderma reesei*, *Neurospora crassa*, and *Aspergillus nidulans*. The amino acid sequences were aligned using ClustalW, and a neighbor-joining tree was generated with 1000 bootstrap replicates using the program MEGA v7.0. Bootstrap values (percentages of 1000 bootstrapped tree replications) greater than 66 are displayed at the nodes.

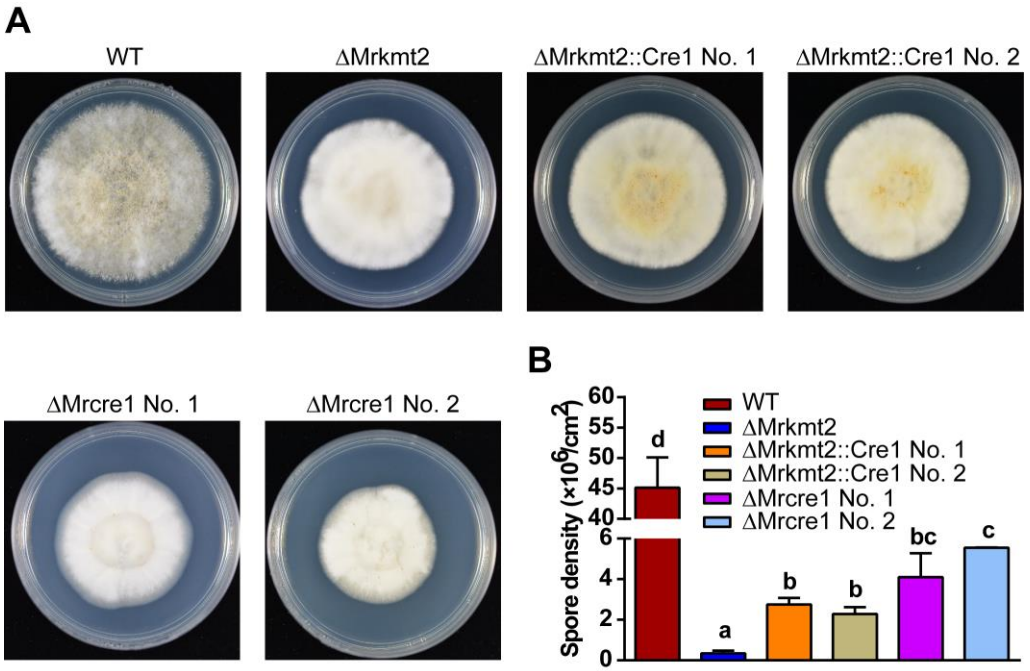

Fig. S8. Overexpression of *Mrcre1* in ΔMrkmt2 rescues sporulation defects.(**A**) Fungal growth assay. The fungal strains were grown on PDA plates for 12 d. (**B**) Comparison of conidia production of the WT and mutants after 12-d growth on PDA. Data are shown as mean ± SD of three technical replicates. Experiments were repeated three times with similar results. Columns labeled with different lowercase letters showed significant differences (Student's *t*-test at $P < 0.05$).

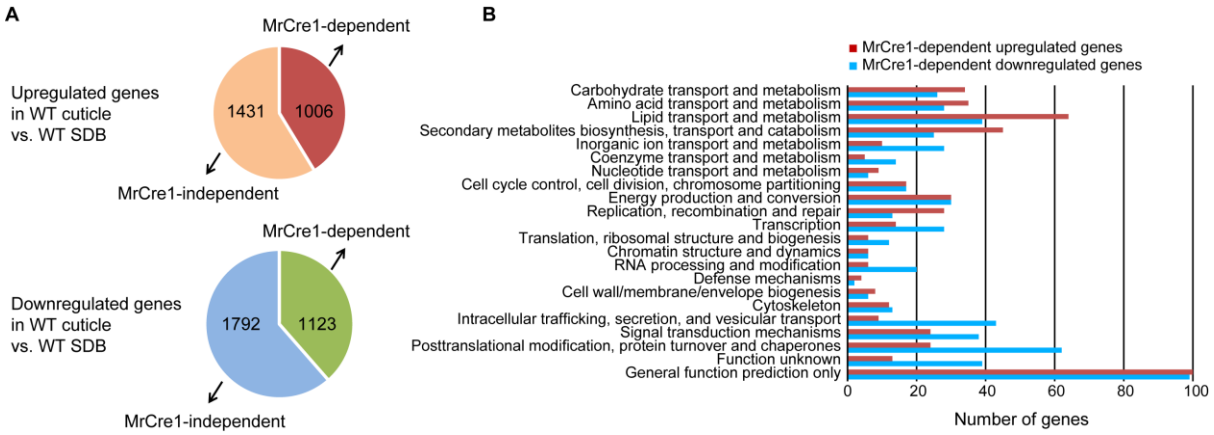

Fig. S9. Global transcriptional analysis of WT and ΔMrcre1 strains grown in the SDB and MM medium supplemented with 0.8% locust cuticle. (**A**) Schematic diagram showing the number of differentially expressed genes (DEGs) after cuticle induction in an MrCre1-dependent manner. Based on the comparison of FC values (fold-change values of gene expression level in the cuticle-induced culture relative to the SDB culture) between the WT and ΔMrcre1 strains, MrCre1-dependent genes were identified when the rate of FC increase or decrease in the ΔMrcre1 strains was less than 50% that of the WT; the remaining genes were classified as MrCre1-independent. (**B**) KOG functional classification of MrCre1-dependent upregulated and downregulated genes.

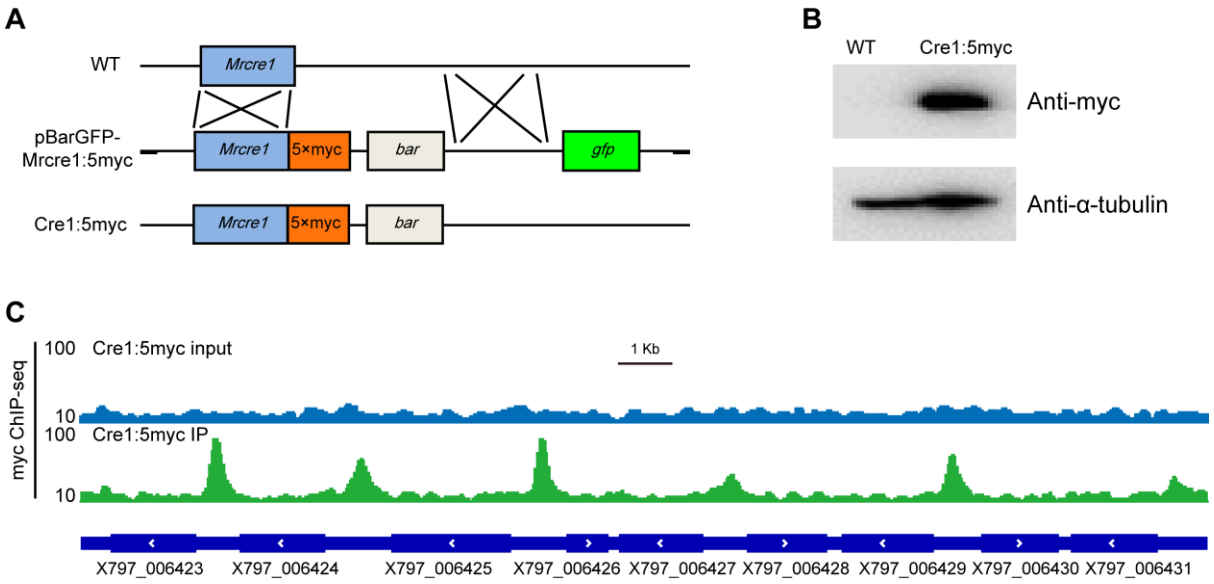

Fig. S10. Gene tagging and ChIP-seq of Cre1:5myc. (**A**) Construction of Cre1:5myc in *M. robertsii* ARSEF 2575. Gene tagging was accomplished by inserting a sequence encoding 5×myc tag at the native genomic locus of the *cre1* gene in the WT strain. The plasmid pBarGFP-Mrcre1:5myc containing two regions identical with the *Mrcre1* reading frame and downstream sequences was used for 5×myc tag insertion by homologous recombination through a double crossover event. (**B**) Western blot demonstrating the production of 5×myc-tagged Cre1. Cre1 C-terminally 5×myc-tagged was successfully detected in the Cre1:5myc strain using an anti-myc antibody. The α-tubulin antibody was used to detect α-tubulin as a positive control. The blots are representative of two replicates. (**C**) Representative genome browser view shows enrichment of Cre1:5myc binding signals from ChIP-seq data.

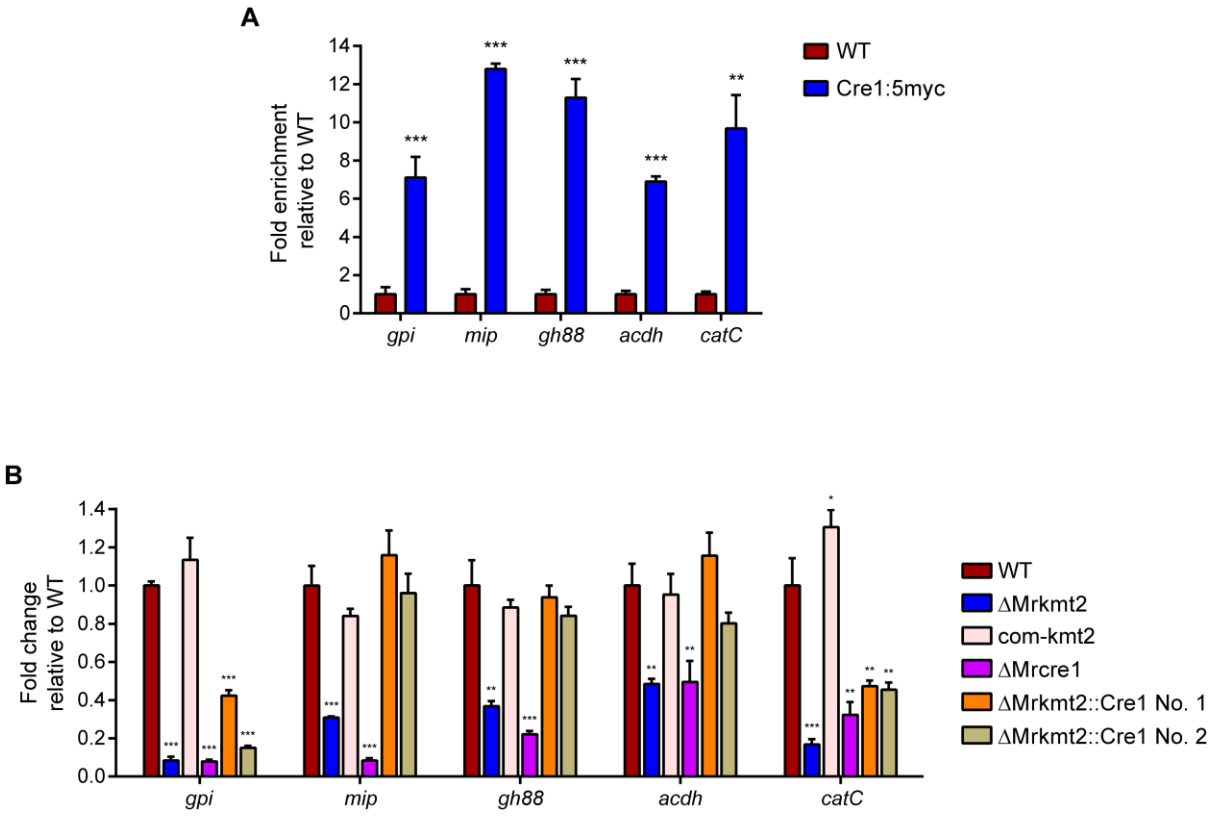

Fig. S11. The other five targets of the transcription factor MrCre1. Genes encoding GPI-anchored protein (*gpi*), MIP family transporter (*mip*), GH88 glycosidase (*gh88*), acyl-CoA dehydrogenase (*acdh*), and catalase C (*catC*) are the direct targets of the transcription factor MrCre1. (**A**) ChIP with quantitative PCR (ChIP-qPCR) validation of MrCre1 binding to the promoters of *gpi*, *mip*, *gh88*, *acdh*, and *catC* genes in the Cre1:5myc strain, shown as a fold-enrichment of the signal from immunoprecipitation over the relative input DNA. WT was used as the negative control. (**B**) qPCR analysis of the *gpi*, *mip*, *gh88*, *acdh*, and *catC* gene expression in different strains grown in the MM medium supplemented with 0.8% locust cuticle; actin was used as a reference gene. Data are shown as mean ± SD of three technical replicates. Double and triple asterisks represent significant differences compared to that in WT determined by Student's *t*-test at $P < 0.01$ and $P < 0.001$, respectively. Experiments were repeated three times with similar results.

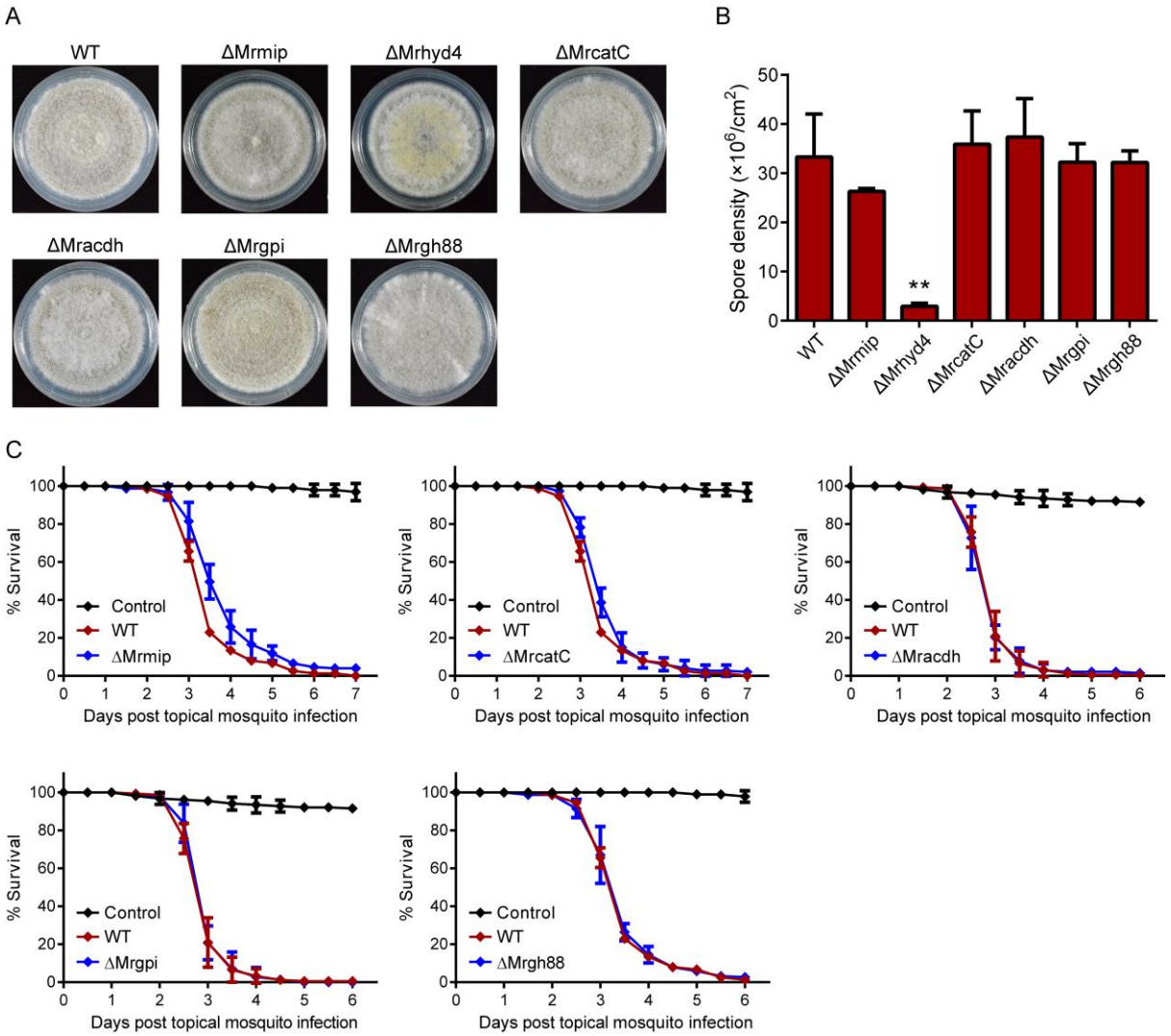

Fig. S12. Effects of deletion of each Cre1 direct target gene on fungal growth, conidiation, and virulence. (**A**) The fungal strains were grown on PDA plates for 12 d and colony morphology was observed. (**B**) Comparison of conidia production of the WT and mutants after 12-d growth on PDA. Data are shown as mean ± SD of three technical replicates. Experiments were repeated three times with similar results. Columns labeled with double asterisks represent significant differences (Student's *t*-test at $P < 0.01$) compared with the WT. (**C**) Survival of *A. stephensi* female adults following topical application with conidial suspensions (1×10^7 conidia/mL) of WT, ΔMrgpi, ΔMrmip, ΔMrgh88, ΔMracdh, and ΔMrcatC strains is shown. Control mosquitoes were treated with 0.01% Triton X-100. Each treatment was replicated three times, with 50 mosquitoes per replicate. Data are shown as mean ± SD of three technical replicates. Experiments were repeated two times with similar results.

Supplementary Table

Table S1. Primers used in this study.

Primers	5'-3' sequences	Applification
Mrkmt2-LF	AGCACTATCTGAGACCTTCACGTA	construction of plasmids for gene deletion
Mrkmt2-LR	GCGGGTAGATCCTCATTCACT	
Mrkmt2-RF	GACCATTCGCTATCGTGACTCTAA	
Mrkmt2-RR	GTCCCAATCCTCGGGCTAT	
Mrcre1-LF	GGAGTAGGAGATGACGACAAGG	
Mrcre1-LR	AAGGCAGCGACGTTCAGATA	
Mrcre1-RF	GGATACAGCAACAGTGGCAGA	
Mrcre1-RR	CCAGGCGAGACAATCAGTTG	
Mrmip-LF	GTTGGTGGGTGTTGGTGGTA	
Mrmip-LR	CCGATGCCGATTACTTACGC	
Mrmip-RF	TGCCCGAAACGCAGTCA	
Mrmip-RR	GCAGAGGAAACTACCGCTGTTA	
Mrhyd4-LF	GATTTCCTAGCATTCCCGCT	
Mrhyd4-LR	TGAGAGAATGTTGCTGTTGTGAG	
Mrhyd4-RF	GGAATTGTTGGAGAAGCTAGTCAG	
Mrhyd4-RR	GTTCGTCATTATCCGATGAGTGTA	
MrcatC-LF	TGTGCTTTCCTACCTGCTGTG	
MrcatC-LR	ACCCTCCCGATACATCCGA	
MrcatC-RF	GGATGAGTTCAGGACAGGAGGA	
MrcatC-RR	ATCTCCGTTGTTGAAATTAGCG	
Mracdh-LF	TTCCCACTGTATTGTTGTTCCAC	
Mracdh-LR	TCCCGACTAAAGTAGTTGATTGC	
Mracdh-RF	TGTTGGTGTAAAGAGGGGTCG	
Mracdh-RR	AGGGCGTGGAGGAGAATAGA	
Mrgpi-LF	CGAAGACTTGGCTGACTGGA	
Mrgpi-LR	GAGTGGCCAATACTGGCG	
Mrgpi-RF	GGAGTTAATACTTGGACTGGCATAGA	
Mrgpi-RR	ACTACAGCCTTGCTTAGGTTCGT	
Mrgh88-LF	AGGACTTGAGCGCCCAGTAC	
Mrgh88-LR	AAGGGCGGATGCACAACTA	
Mrgh88-RF	TGCTGTATTTCGGATGCCA	
Mrgh88-RR	TCGCCATAGTCCCACCACT	
com-kmt2-F	AGCACTATCTGAGACCTTCACGTA	construction of plasmids for gene complementation
com-kmt2-R	CGTCAATATGAAGTGATGACGGT	
com-cre1-F	GGAGTAGGAGATGACGACAAGG	
com-cre1-R	TTGTCGGCGTGCTATTATTCC	
overexpression-cre1-F	ACATGCAACGGTCACAGTCTG	construction of Cre1 overexpression plasmid
overexpression-cre1-R	AACCCGGTCCATCAGATCG	
Cre1:5myc-LF	ACATGCAACGGTCACAGTCTG	construction of Cre1:5myc plasmid
Cre1:5myc-LR	AACCCGGTCCATCAGATCG	
Cre1:5myc-RF	GACAAGATTCGACCAAGTCCAC	
Cre1:5myc-RR	CCTGCGATTTGATGTTTCTCC	
Mrkmt2-qPCR-F	TCTGAACTCATTCGGTACCCAA	qPCR
Mrkmt2-qPCR-R	TCTGTATATGTCGGTTTGGAACTCT	
Mrcre1-qPCR-F	TCGCTTCACCATAACACGACA	
Mrcre1-qPCR-R	GTCAGGGACATTCCATTGCTC	
Mrmip-qPCR-F	TGCCGTCTACTGGATCCTCAA	
Mrmip-qPCR-R	TGCGGTGGTTCTTCTGGTG	
Mrhyd4-qPCR-F	AGCACAAGAAGCCTCACCCT	

Mrhyd4-qPCR-R	AGAAGGCCGTCGAGGACA	
MrcatC-qPCR-F	AATCTTGACCCGCATCTCG	
MrcatC-qPCR-R	TGAATACAAAGTCTTGCACGCC	
Mracdh-qPCR-F	CAGGAGGCCGACTTGAAACT	
Mracdh-qPCR-R	CCCATTGCCACCAAACAGTAA	
Mrgpi-qPCR-F	CCTGTGCCGACATCACCTAC	
Mrgpi-qPCR-R	GGCGGGCTTGTCCTTTTC	
Mrgh88-qPCR-F	CGGGATGCTCGTGATTTCC	
Mrgh88-qPCR-R	CATAGCACAACGCCAGGGT	
Mrm24-qPCR-F	GCTGGTGAATCTGGTGCCA	
Mrm24-qPCR-R	AACTGACGGAGGTTCGGTCTG	
Mrs28-qPCR-F	CATCCTCGAGCACCGCTACT	
Mrs28-qPCR-R	AAGTGGACGAGGTCCTGGATG	
Mrmpl1-qPCR-F	CCTTACAACAAGAGTATCGAGGGC	
Mrmpl1-qPCR-R	CTGACGACAAAGGCGGTAGAG	
MrrgsA-qPCR-F	ACCCTCCATCTCAGGAAAGCA	
MrrgsA-qPCR-R	GACCGCTAGGCAGACTTAGGAG	
MratfB-qPCR-F	CAAGGTCACCAACAATACAATCG	
MratfB-qPCR-R	GACATTTTGAAGCGGCAACAC	
Mrtf1-qPCR-F	AGATAGCCGATGAGTGCCGTTA	
Mrtf1-qPCR-R	CCGATTAGAATAATCGTCGTGC	
Mrgpd-qPCR-F	CCCAGAACATCATTCCCAGC	
Mrgpd-qPCR-R	TCAATGCGGGCAGTCAAGTC	
Mractin-qPCR-F	GCTCCCATCAACCCCAAGT	
Mractin-qPCR-R	ACGACCAGAGGCGTAAAGAG	
Mrcre1-ChIP qPCR-F	TCGCTGCCTT TGAGACTAACACT	ChIP qPCR
Mrcre1-ChIP qPCR-R	ATTCAGCAAGTTGGTGAAGTCG	
Mrmip-ChIP qPCR-F	GGAATGCAGGGATCTCGAATA	
Mrmip-ChIP qPCR-R	CTCCACCGGATCGGACTGT	
Mrhyd4-ChIP qPCR-F	AGCACAAGAAGCCTCACCCT	
Mrhyd4-ChIP qPCR-R	AGAAGGCCGTCGAGGACA	
MrcatC-ChIP qPCR-F	CTTGTCCCGCGAAGCTATTG	
MrcatC-ChIP qPCR-R	ACCCTCCCGATACATCCGA	
Mracdh-ChIP qPCR-F	TCGGGAGTCCTAGCTGGCAT	
Mracdh-ChIP qPCR-R	CGTATAGGGTGCGTGACTAACAAT	
Mrgpi-ChIP qPCR-F	GCAACCGTGTAGGCAAGGAG	
Mrgpi-ChIP qPCR-R	GAGAAGTGCAAGCAACCCTGT	
Mrgh88-ChIP qPCR-F	ATCGAGACTGCTTTCGAGACAA	
Mrgh88-ChIP qPCR-R	TCCTTACCCAGCGGGACACT	
Mrm24-ChIP qPCR-F	GCTGGTGAATCTGGTGCCA	
Mrm24-ChIP qPCR-R	AACTGACGGAGGTTCGGTCTG	
Mrs28-ChIP qPCR-F	CATCCTCGAGCACCGCTACT	
Mrs28-ChIP qPCR-R	AAGTGGACGAGGTCCTGGATG	
Mrmpl1-ChIP qPCR-F	TACTCGCCTCACTCACGTCCA	
Mrmpl1-ChIP qPCR-R	GCCATTGACCTGAGGGACAG	
MrrgsA-ChIP qPCR-F	CGGCTCCACCAGTTACGACA	
MrrgsA-ChIP qPCR-R	TTGGCTAGGCACCGAATAAGA	
MratfB-ChIP qPCR-F	CAAGGTCACCAACAATACAATCG	
MratfB-ChIP qPCR-R	GACATTTTGAAGCGGCAACAC	
Mrtf1-ChIP qPCR-F	AGATAGCCGATGAGTGCCGTTA	
Mrtf1-ChIP qPCR-R	CCGATTAGAATAATCGTCGTGC	

F, forward; R, reverse.